nature plants

ARTICLES

DOI: 10.1038/s41477-017-0021-9

In vivo gibberellin gradients visualized in rapidly elongating tissues

Annalisa Rizza[1], Ankit Walia[1], Viviane Lanquar[2], Wolf B. Frommer[2,3,4]* and Alexander M. Jones[1,2]*

The phytohormone gibberellin (GA) is a key regulator of plant growth and development. Although the upstream regulation and downstream responses to GA vary across cells and tissues, developmental stages and environmental conditions, the spatiotemporal distribution of GA in vivo remains unclear. Using a combinatorial screen in yeast, we engineered an optogenetic biosensor, GIBBERELLIN PERCEPTION SENSOR 1 (GPS1), that senses nanomolar levels of bioactive GAs. *Arabidopsis thaliana* plants expressing a nuclear localized GPS1 report on GAs at the cellular level. GA gradients were correlated with gradients of cell length in rapidly elongating roots and dark-grown hypocotyls. In roots, accumulation of exogenously applied GA also correlated with cell length, intimating that a root GA gradient can be established independently of GA biosynthesis. In hypocotyls, GA levels were reduced in a *phytochrome interacting factor* (*pif*) quadruple mutant in the dark and increased in a phytochrome double mutant in the light, indicating that PIFs elevate GA in the dark and that phytochrome inhibition of PIFs could lower GA in the light. As GA signalling directs hypocotyl elongation largely through promoting PIF activity, PIF promotion of GA accumulation represents a positive feedback loop within the molecular framework driving rapid hypocotyl growth.

Gibberellins (GAs) are plant hormones that promote organ growth in a variety of developmental contexts and mutants defective in GA biosynthesis are characterized by reduced elongation of roots, stems and floral organs[1]. Although GA was first discovered as a plant growth regulator nearly a century ago (reviewed here[2]), knowledge of GA distribution at the cellular level remains limited by an inability to quantify GA in vivo. Reporter constructs driven by the promoters of GA biosynthetic enzymes have revealed dynamic expression maps over development[3–5], suggesting that spatiotemporal distribution of GA is tightly regulated. However, inference of GA distribution from enzyme expression profiles is complicated when GA isozymes exhibit contrasting expression patterns, for example during hypocotyl de-etiolation where expression of *AtGA3ox1* decreases over sixfold while *AtGA3ox2* increases 16-fold[6]. Furthermore, GA distributions are also regulated by catabolism, conjugation and, because GAs are mobile signals, transport steps[1]. Although overall GA levels can be quantified directly with biochemical methods, such as gas chromatography/mass spectrometry[7], these approaches average over many cells and do not enable dynamic analyses.

In primary root tips, where GA deficiency reduces cell elongation and cell proliferation rate leading to shorter roots, the biological function of GA in the *Arabidopsis* root has received considerable attention[8–13]. Ubeda-Tomás et al. (2008) found that blocking GA signalling specifically in the endodermis is sufficient to disrupt GA-directed cell elongation in the *Arabidopsis* root, indicating that the endodermis is a key site of GA action in root elongation[11]. This hypothesis is supported by Shani et al. (2013), who observed accumulation of exogenous fluorescein-GA_3 and fluorescein-GA_4 over time in the vacuoles of endodermal cells of the elongation zone[13]. However, a multi-scale model of the relationship between GA distribution and root cell growth proposed by Band et al. (2012) posits that cellular GA levels decrease—owing to cytosolic dilution—as cells progress through the root elongation zone[9]. Despite such investigations using cell-specific genetic intervention into GA signalling[11], fluorescein labelled GAs[13] and multi-scale modelling of GA levels[9], the distribution of GA in roots remains unclear.

In several tissues, GA levels are altered in response to environmental stimuli, and this redistribution of GA is critical for key developmental transitions such as germination, photomorphogenesis and the transition to flowering[1]. For example, in *Arabidopsis* seeds, light stimuli trigger activation of the phytochrome photoreceptors (PHYs), leading to elevated GA levels, which promote germination[14,15]. Interestingly, in hypocotyls the opposite is true, as light signalling lowers GA levels and the cessation of the rapid elongation observed in darkness[16–18]. In seeds, phytochromes raise GA levels in part through relieving PHYTOCHROME INTERACTING FACTOR (PIF) mediated inhibition of GA accumulation[19]. In the case of the hypocotyl, it remains unclear how light signalling lowers GA levels or how elevated GA levels are promoted by darkness. Also, the distribution of GA in hypocotyls is yet unknown.

Here we used an optogenetic biosensing approach, based on a Förster Resonance Energy Transfer (FRET) biosensor for GA for high-resolution quantification of spatiotemporal GA distribution. Small molecule FRET biosensors that directly interact with and report on ligand concentration have been used in living plants to generate high-resolution measurements of calcium[20,21], sugars[22,23] and the plant hormone abscisic acid[24,25]. In these synthetic fusion proteins, binding of the ligand to a sensory domain induces structural rearrangements that alter the amount of energy transfer between a donor fluorescent protein moiety and an acceptor fluorescent protein moiety. Sensor output can be tracked by exciting the donor and measuring the ratio of acceptor emission over donor emission; this emission ratio is independent of biosensor expression levels and is proportional to ligand concentration[26]. Compared with gas chromatography/mass spectrometry, optogenetic biosensors that directly report on small molecule concentrations are minimally invasive, provide high-resolution and require only light inputs once the biosensor is expressed in vivo[26].

[1]Sainsbury Laboratory, Cambridge University, Cambridge, UK. [2]Carnegie Institution for Science, Department of Plant Biology, Stanford, CA, USA. Present address: [3]Institute for Molecular Physiology, Heinrich Heine Universität, 40225 Düsseldorf, Germany. [4]Max Planck Institute for Plant Breeding Research, 50829 Cologne, Germany. *e-mail: frommew@hhu.de; alexander.jones@slcu.cam.ac.uk

To develop and optimize a FRET biosensor for GA, we used plant hormone receptors as sensory domains. GIBBERELLIN INSENSITIVE DWARF 1 (GID1) proteins are soluble receptors that interact with GA in an internal binding pocket[27]. GA binding promotes GID1 interaction with members of the DELLA family of growth regulators. The GID1-GA complex binds the N-terminal DELLA domain, which leads to the degradation of the DELLA protein after ubiquitination of the C-terminal GRAS domain[28]. We endeavoured to co-opt the *Arabidopsis* GA perception machinery into a conformationally dynamic GA binding domain within a FRET biosensor by fusing GID1 variants to DELLA N termini. Such a fusion would effectively convert GA-dependent intermolecular interactions into GA-dependent intramolecular structural rearrangements.

We systematically screened potential biosensor constructs in order to identify GIBBERELLIN PERCEPTION SENSOR 1 (GPS1). GPS1 functions as a biosensor for GA that responds with an increase in emission ratio to nanomolar concentrations of bioactive GAs.

Here we show that, when expressed in *Arabidopsis* and targeted to cell nuclei, GPS1 reports GA distribution and gradients in vivo in multiple tissues and growth conditions both in wild-type and light signalling mutants[29].

Results

Combinatorial screen for optimized FRET-based GA biosensors. Engineering FRET biosensors is a semiempirical process that often requires the screening of ligand binding domains fused to pairs of FRET donor/acceptor variants to identify fusion proteins that exhibit ligand-induced changes in FRET (Fig. 1a[26]). Here we used a combinatorial FRET biosensor cloning approach in which a series of Gateway Entry clones coding for potential GA binding domains were recombined with a set of previously designed Gateway destination vectors (pDR-FLIPs) which carry fluorescent protein gene variants capable of FRET[24].

A matrix of 24 potential GA binding domain constructs were generated as Gateway Entry clones. GA binding domains were derived from AtGID1A, B or C linked via a flexible 12-amino acid linker (L12) to either the N or C terminus of two different truncations of the DELLA proteins AtRGA or AtGAI. These 24 candidates were recombined with a Gateway Destination vector (pDR-FLIP39[24]) that encodes enhanced dimerization (ed) variants of Aphrodite (edAFP) as FRET acceptor and edeCFP as FRET donor. We screened fusion proteins expressed in protease-deficient yeast[30] for GA-dependent alterations in the fluorescence emission curves after FRET donor excitation at 430 nM (donor excitation (Dx); Supplementary Fig. 1a). For two of the 24 fusion proteins, GA_3 triggered an increase in emission at 535 nm (donor excitation acceptor emission, DxAm) and a concomitant decrease in emission at 485 nm (donor excitation donor emission, DxDm), characteristic of a FRET biosensor with a positive ratio change (ΔDxAm/DxDm). We next sought to optimize the ratio change and fluorescent proteins of one of these fusion proteins by combinatorially screening a series of variants of the L12 linker and a series of FRET pair variants (Supplementary Fig. 1b). This screen resulted in an optimized biosensor, named GPS1, which consisted of an N-terminal edAFP linked via the translated attB1 to a 74-amino acid truncation of AtGAI linked via L12 to AtGID1C linked via the translated attB2 site to edCerulean (Fig. 1b). On the basis of the crystal structure of AtGID1A in complex with AtGAI and our observed DxAm/DxDm values for GPS1 (hereafter referred to as GPS1 emission ratio) with and without GA_3 (Fig. 1c), one hypothesis is that GPS1 switches from a moderate FRET to high FRET average state upon binding to GA.

Generation of the non-responsive control GPS1-NR. Non-responsive variants of GPS1, as important controls for interpretation of GPS1-derived in vivo data, were generated via mutation of AtGID1C residues involved in GA binding and AtGAI residues involved in interaction with GID1 proteins. GPS1-S114A/F115A carries two alanine substitutions in the GA binding pocket of AtGID1C based on corresponding mutations in the rice GID1 protein that had been shown to disrupt GA binding[27]. GPS1–S114A/F115A shows no detectable response to GA in vitro (Fig. 1e). In GPS1-E51K/E54R, the substitution of two positively charged residues for negatively charged residues in AtGAI likely disrupts two salt-bridges that function in the interaction with AtGID1[31]. By combining the AtGID1C-S114A/F115A mutant with the AtGAI-E51K/E54R mutant, we generated a mutant biosensor (termed GPS1-non-responsive, GPS1-NR) that is apparently non-responsive to GA and, importantly, whose component GAI domain is predicted to be deficient in in planta interactions with endogenous GAI binding factors including GIDs (Fig. 1e).

Characterization of GPS1. To determine the dynamic range of GA detection by GPS1, we measured the dissociation constant (K_d) of metal-affinity purified GPS1 in vitro by tracking dose-dependent changes in GPS1 emission ratios for several bioactive, precursor and catabolized GAs (Fig. 2a,b). It had been shown that the K_d of AtGID1C for 16,17-dihydro-GA_4 is 1.9 μM and that the K_d decreases to 46 nM in the presence of AtGAI[32], indicating that AtGAI increases AtGID1C affinity for GA 50-fold. The K_d of GPS1, which contains full-length AtGID1C and the DELLA domain of AtGAI, was 24 nM for GA_4 (Fig. 1b). This affinity is comparable with the AtGID1C affinity for GA_4 in the presence of AtGAI[32]. The K_d of GPS1 for GA_1 was 110 nM and for GA_3 was 240 nM. Overall, GPS1 was responsive to several GAs (Fig. 2a,b), with lower affinities relative to GA_4, consistent with the properties of unfused GID and GAI[32]. We examined whether GA binding by GPS1 is reversible by treating GPS1 with different GAs, performing two 20 minute steps of buffer-exchange chromatography, and then treating with GA a second time. GPS1 was partially reversible for GA_1 and GA_3 but not for GA_4 (Fig. 2c). Because the GPS1 response to GA_4 remains even after removal of GA_4 from solution, GPS1 emission ratio change is likely unable to report rapid GA depletion in vivo.

Expression of GPS1 in planta. To assess GA distribution in planta, we generated stable transgenic *Arabidopsis* lines expressing a nuclear targeted variant of GPS1 (nlsGPS1) under the control of a promoter fragment previously shown to direct a broad expression pattern (p16[33]). Targeting the biosensor to the nucleus allowed for analysis of GA accumulation in the compartment most relevant to endogenous GA perception and facilitates comparison of GPS1 emission ratios between neighbouring cells. The use of the p16 promoter led to successful expression of GPS1 transgenes in both roots and shoots of wild-type Col-0 *Arabidopsis*. Importantly, GPS1 expression did not result in detectable phenotypic changes in GA-dependent hypocotyl or root growth (Supplementary Fig. 2a,b). We further analysed whether the presence of GPS1 might interfere with GA-dependent seedling growth by comparing nlsGPS1 or GPS1 with wild-type Col-0 in response to treatment with the GA biosynthesis inhibitor paclobutrazol (PBZ) alone or in combination with GA_4 (Fig. 2d and Supplementary Fig. 2c). All lines exhibited an expected reduction in hypocotyl elongation in presence of PBZ that was gradually reversed by increasing concentrations of GA_4. However, nlsGPS1 and GPS1 seedlings were hyposensitive to PBZ treatment (Fig. 2d and Supplementary Fig. 2c), a phenotype that might be due to increased GA sensitivity resulting from overexpression of the full length AtGID1C moiety of the GPS1 biosensor. Similar hormone hypersensitivity had been observed for *Arabidopsis* lines expressing ABACUS1 biosensors[24]. The increased GA sensitivity resulting from expression of the GPS1 biosensor, although not apparent under normal growth conditions, must be considered when interpreting results from all analyses. Thus, further

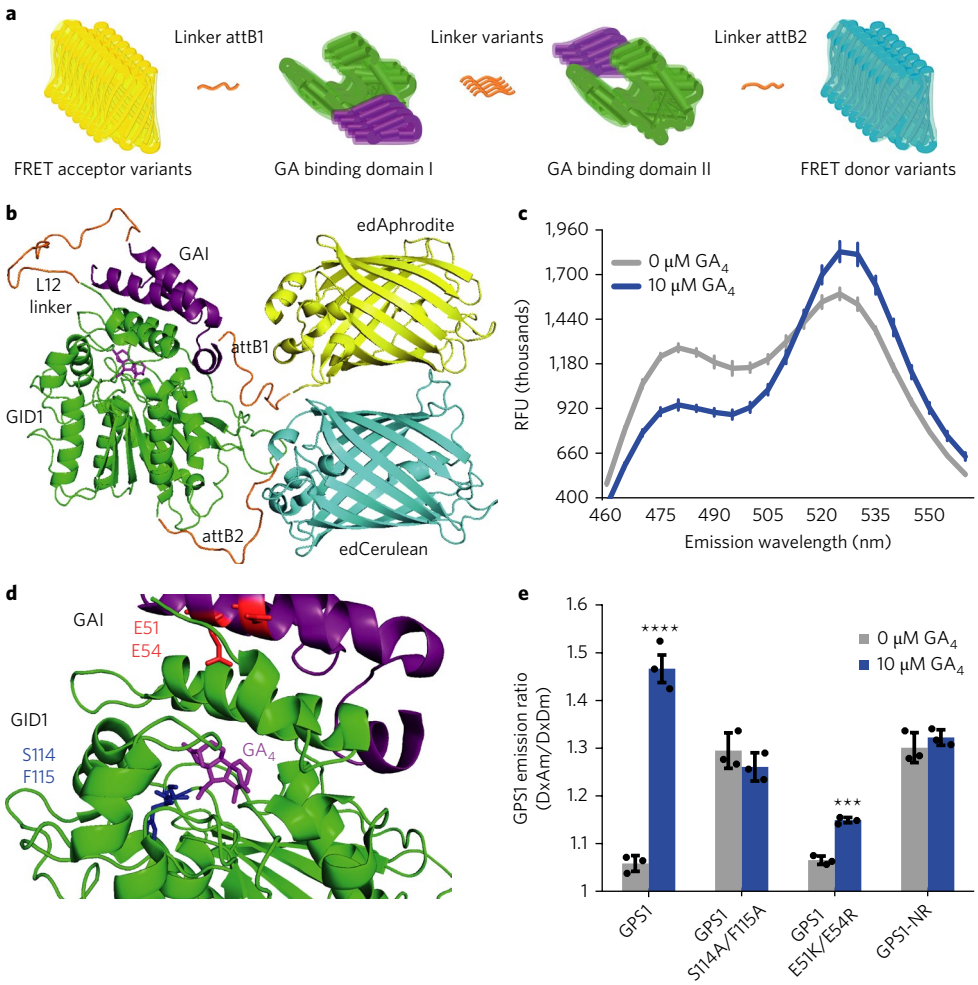

Fig. 1 | Engineering and GA response of GPS1 and GPS1-NR. a, Representation of variant domains included in potential FRET biosensors for GA: GA binding domain variants (GA binding domain I and II connected through linker variants) were fused via attB1 and attB2 linkers to fluorescent protein FRET pairs (variant donor and acceptor fluorescent proteins). **b**, Structural model of GPS1 bound to GA_4. The GID1C protein (green), GAI truncation (purple) and GA_4 (magenta) representations are from a published structure of an AtGID1A, AtGAI truncation, GA_4 ternary complex (PDB 2ZSI[31]). The edAphrodite (yellow) representation is from a published structure of Venus (PDB 1MYW[55]) and the edCerulean representation is from a published structure of Cerulean (PDB 2WSO[56]). The representations of three linkers (translated attB1, L12 and translated attB2) were built in PyMol software. **c**, Fluorescence emission curve of purified GPS1 protein with and without GA_4 treatment. **d**, The GPS1 residues of the GAI and GID1 domains mutagenized to make GPS1-NR construct are highlighted in red and blue, respectively. **e**, Fluorescence emission ratio of purified GPS1, GPS1-S114A/F115A, GPS1-E51K/E54R and GPS1-NR proteins with and without GA_4 treatment. **c**,**e**, Student's t-test ****P value < 0.0001, ***P value < 0.001. Means and s.d. of three replicates are presented. Complete experiments were repeated at least three times with similar results. RFU, relative fluorescence units.

engineering is required to create GA biosensors with reduced interactions with endogenous machinery as was accomplished in the second generation of chameleon calcium sensors[34].

Live-cell imaging of GPS1 response to endogenous GAs in roots. To explore whether GPS1 is suitable for measuring GA distribution in plants, we investigated nlsGPS1 emission ratios in roots of *Arabidopsis* seedlings grown on agar plates and exposed to long-day cycling (16 h light/8 h dark) for three days (hereafter referred to as 'light-grown', Fig. 3, Supplementary Fig. 3). GA signalling in roots is required for meristem size and cell elongation[11,12]. In roots, we observed an apparent gradient of GA with low nlsGPS1 emission ratios in the apical cell division zone transitioning to increasing nlsGPS1 emission ratios in the elongation zone (Fig. 3a). Although local variation was observed, mean nlsGPS1 emission ratios increased significantly along the root growth axis (Fig. 3b). Interestingly, the increase in nlsGPS1 emission ratios in the elongation zone was observed in epidermal and cortical cells and was not limited to the endodermis (Fig. 3c,d), which is thought to be a main site of action for GA signalling in root elongation[11]. To evaluate whether nlsGPS1 emission ratios report actual GA distribution, we analysed emission ratios in seedlings expressing nlsGPS1-NR that do not respond to GA. These plants showed low emission ratios in all root zones with a small but significant increase from the division zone to the elongation zone (Fig. 3a,b). However, the difference in emission ratios between the division zone and the late elongation zone is small (mean difference = 0.13) when compared with nlsGPS1 (mean difference = 0.89), implying that the gradient in nlsGPS1 emission ratios along the root growth axis is not artefactual (Fig. 3b). We also observed greatly reduced nlsGPS1 emission ratios in roots of a *ga3ox1, ga3ox2* double mutant (Fig. 3a,b), as one might expect for a mutant with greatly reduced GA levels[4]. GA signalling results in proteasome mediated degradation of DELLAs[35]. We assessed the distribution of the DELLA protein AtRGA through imaging *Arabidopsis* lines expressing a pRGA::GFP-RGA translational fusion (ref. [35], Supplementary Fig. 4) and observed pRGA::GFP-RGA

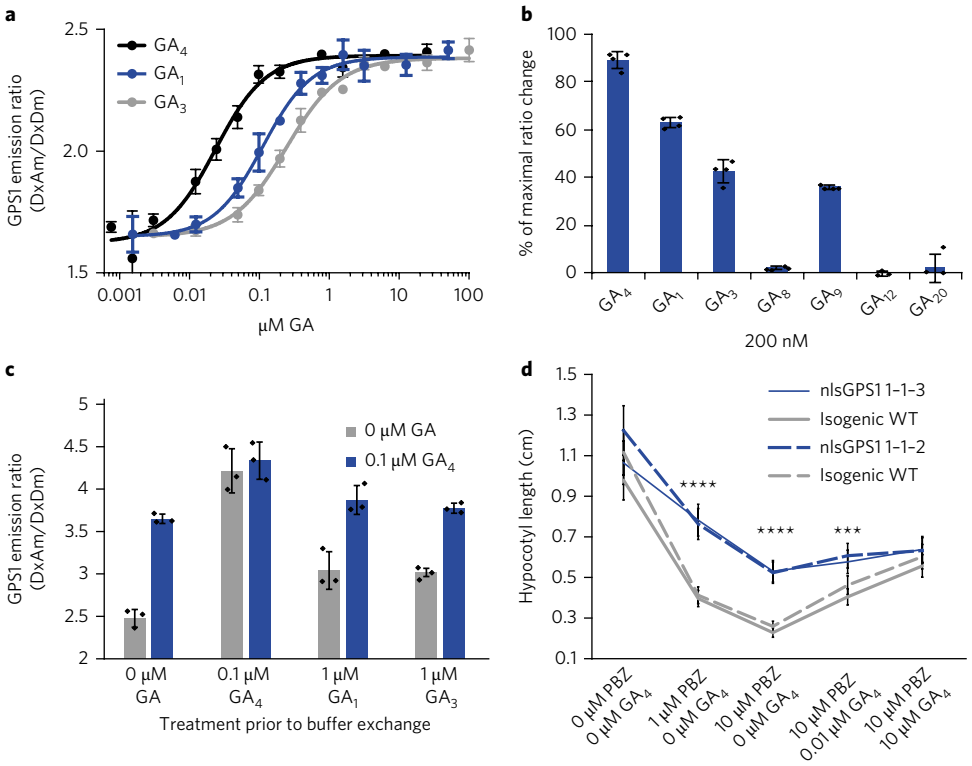

Fig. 2 | Fluorescence emission ratio response of purified GPS1 to GAs. a, GPS1 fluorescence response to increasing concentrations of bioactive GAs (GA_4, GA_1 or GA_3). **b**, Percent maximal ratio change of GPS1 in response to 200 nM GAs. **c**, GPS1 emission ratio response to a second GA treatment (0.1 μM GA_4) after a prior GA treatment and 2x buffer exchange. Means and s.d.'s of three replicates are presented. Complete experiments were repeated at least three times with similar results. **d**, Hypocotyl lengths of two nlsGPS1 lines were compared with wild-type Col0 siblings (isogenic) with and without Paclobutrazol (PBZ) (1 μM and 10 μM) and GA_4 (0.01 μM and 10 μM) treatments. Student's *t*-test, ****P value < 0.0001, ***P value < 0.001. At 1 μM PBZ and 0 μM GA_4: solid lines Cohen's $d = 5.92$, dashed lines Cohen's $d = 6.04$. At 10 μM PBZ and 0 μM GA_4: solid lines Cohen's $d = 6.50$, dashed lines Cohen's $d = 7.31$. Means and s.d.'s of three replicates are presented. Complete experiments were repeated at least three times with similar results.

protein distribution to be anticorrelated with nlsGPS1 emission ratios in roots (Supplementary Fig. 4a). Taken together, the distribution of pRGA::GFP-RGA fluorescence and nlsGPS1 emission ratios indicate that GA levels correlate with cell length in *Arabidopsis* roots (Fig. 3).

Live-cell imaging of GPS1 response to exogenous GAs in roots. Plants translocate GAs[36] from source to sink tissues during normal development to trigger responses such as stem growth and flowering[37–40]. Indicative of GA's role as a mobile signal, a variety of plant tissues have been shown to accumulate and respond to exogenously supplied GAs[38]. Treatments of *Arabidopsis* roots with fluorescein-GA_3 and fluorescein-GA_4 resulted in dye accumulation first in all cells of the elongation zone before subsequent concentration in vacuoles of the endodermis in the elongation zone[13]. However, it remains unclear which cells and cell types are competent in accumulating unmodified GAs. We analysed nlsGPS1 emission ratios in roots of *Arabidopsis* seedlings before and 20 minutes after treatment with exogenous GA_4, GA_1 and GA_3 at concentrations ~40-, 90- and 40-fold higher than the respective GPS1 K_d (Fig. 4a–d, Supplementary Fig. 5a). Treatment of *Arabidopsis* roots with exogenously applied GA_1 or GA_3 did not increase nlsGPS1 emission ratios, whereas exogenous GA_4 led to increased nlsGPS1 emission ratios specifically in the elongation zone. Thus, the mechanisms governing accumulation of exogenously applied GAs can effectively discriminate between GAs, and preferentially accumulate GA_4—the dominant bioactive GA in *Arabidopsis*—over GA_3 or GA_1. Similar to endogenous GA, accumulation of exogenous GA_4 was not limited to the endodermis, though it should be noted that following an initial accumulation of exogenous GA_4, nlsGPS1 would not report on depletion of GA from epidermal and cortical cells nor on accumulation of GA in vacuoles.

The accumulation of exogenously applied GAs as detected by nlsGPS1 in the nuclei of root cells results from an ensemble of import activity less depletion activities such as catabolism, compartmentation and export. To quantify this ensemble activity with high spatiotemporal resolution, we performed time-course experiments of *Arabidopsis* roots growing in the RootChip16, a microfluidic device that allows imaging of roots growing in controlled perfusion chambers[23,24]. After 20 minutes of perfusion with GA_4, GA accumulation closely mirrored the gradient of endogenous GA prior to treatment (Fig. 4e,f, Supplementary Video 1). The differential accumulation of exogenous GA across the root could result from differential depletion activity, as had been shown for ABA depletion activities in different zones of *Arabidopsis* roots[24]. Direct analysis of GA depletion rates was not possible due to the low apparent reversibility of GPS1 binding to GA (Fig. 1c). To determine if biosensor turnover could nevertheless lead to a lowering of nlsGPS1 emission ratios to baseline levels, we analysed roots after a 20 minute treatment with 100 nM GA_4 and found that nlsGPS1 emission ratios in GA responsive cells remained high for at least 2 hours and were not highly responsive to a subsequent 20 minute treatment with 100 nM GA_4 (Supplementary Video 1, Supplementary Fig. 5). Consistent with the observation that nlsGPS1 responses are stable in vivo, we did not observe rapid turnover of nlsGPS1 protein in vivo, as would have been indicated by loss of yellow fluorescent protein (YFP) fluorescence intensity, after treatment with the protein synthesis inhibitor cycloheximide for 3 hours (Supplementary Fig. 6).

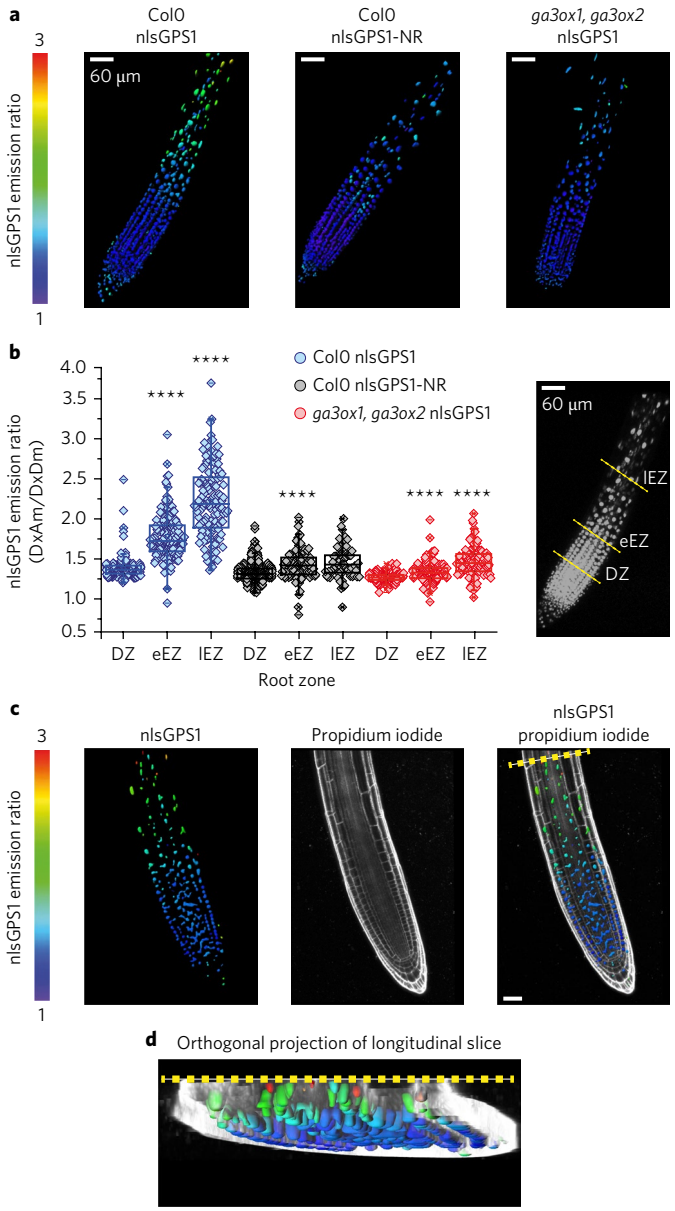

Fig. 3 | Emission ratios of nlsGPS1 in root tips. a, Three-dimensional images of nlsGPS1 or nlsGPS1-NR emission ratios of roots 3 days post sowing in wild-type Col0 or *ga3ox1, ga3ox2* mutant backgrounds. Two independent lines of each genotype are also presented in Supplementary Fig. 3. **b**, Beeswarm and box plot of nlsGPS1 or nlsGPS1-NR emission ratios for nuclei of late division zone (DZ, 100–200 µm from quiescent centre), early elongation zone (eEZ, 200–400 µm from quiescent centre) and late elongation zone (lEZ, 400–800 µm from quiescent centre). Zones indicated graphically in the example image at right ($n > 68$ nuclei from three independent seedlings for each genotype and root zone). For Col0 nlsGPS1, eEZ versus DZ Kruskal-Wallis test ****P value < 0.0001, Cohen's $d = 1.83$; and lEZ versus eEZ Kruskal-Wallis test ****P value < 0.0001, Cohen's $d = 1.16$. For Col0 nlsGPS1-NR, eEZ versus DZ Kruskal-Wallis test ****P value < 0.0001, Cohen's $d = 0.60$; and lEZ versus eEZ Mann-Whitney U test P value = 0.41, Cohen's $d = 0.13$. For nlsGPS1 *ga3ox1, ga3ox2*, eEZ versus DZ Kruskal Wallis test ****P value < 0.0001, Cohen's $d = 0.73$; and lEZ versus eEZ Kruskal-Wallis test ****P value < 0.0001, Cohen's $d = 0.84$. **c**, Longitudinal slice of nlsGPS1 in a Col0 root tip coimaged with PI staining of cell outlines. **d**, Orthogonal projection of the longitudinal slice from **c**. Complete experiments were repeated at least three times with similar results.

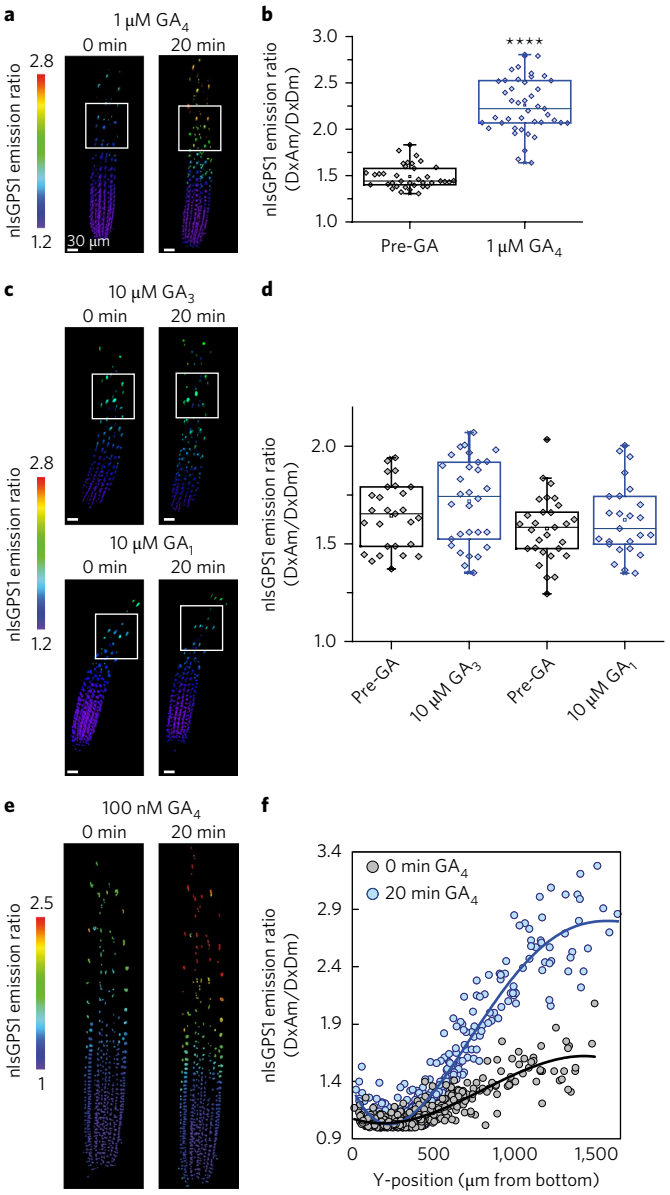

Fig. 4 | Emission ratios of nlsGPS1 in roots before and after treatment with GAs. a,**c**, Three-dimensional images of nlsGPS1 roots before and after GA_4(**a**), and GA_3 and GA_1 treatments (**c**). **b**,**d**, Corresponding beeswarm and box plot of nlsGPS1 emission ratios for nuclei of late elongation zone, 400–600 µm from quiescent centre (region demarcated with frame in **a** and **c**, $n > 24$ nuclei). nlsGPS1 emission ratio was statistically different before and after GA_4 (Student's t-test, ****P value < 0.0001, Cohen's $d = 3.38$). **e**, Still frames from Supplementary Video 1 at 0 and 20 minutes post GA_4 treatment. Seedlings were grown in the RootChip16. **f**, nlsGPS1 emission ratios for individual nuclei before (grey) and after (blue) GA_4 treatment in relation to distance from the root tip (micrometres from bottom). Complete experiments were repeated at least three times with similar results.

An alternative hypothesis is that differential import activity, rather than differential catabolism, results in an accumulation gradient of exogenous GA_4 (Fig. 4e,f). As GAs are mobile, differential import could also contribute to gradients of endogenous GA (Figs. 3 and 4). Band et al. (2012) concluded from analyses of *AtGA2ox* expression patterns and root growth phenotypes of a *ga2ox* quintuple mutant that GA catabolism was likely low in both division and elongation zones[9]. Further investigations are needed to clarify how

spatial regulation of GA enzymes and transporters set cellular GA distribution such that GA levels are correlated with cell length in *Arabidopsis* roots.

Live-cell imaging of GPS1 in stamen filaments. Stamen filaments undergo rapid elongation in order to deposit the pollen from the anther to the stigma[41]. We observed high nlsGPS1 emission ratios compared with nlsGPS1-NR in elongating filaments, indicating that GA levels increase during filament growth (Supplementary Fig. 7). Our results are consistent with the strong expression of *AtGA3ox* biosynthetic enzymes in stamen filaments[3].

Live-cell imaging of GPS1 in light- and dark-grown hypocotyls. Environmental stimuli are known to regulate GA levels in several tissues, for example in basal hypocotyls where light signalling lowers GA leading to slower elongation growth[16–18]. In nuclei of light-grown hypocotyl cells, we observed low nlsGPS1 emission ratios near the shoot apical meristem and variable nlsGPS1 emission ratios in the faster growing central region of the hypocotyl (Fig. 5, Supplementary Fig. 8). As in roots, both wild-type seedlings expressing nlsGPS1-NR and *ga3ox1, ga3ox2* double mutant seedlings expressing nlsGPS1 exhibited reduced emission ratios (Fig. 5a,b), suggesting that the nlsGPS1 emission ratios observed in light-grown, wild-type hypocotyls are indicative of GA distribution. We investigated the relationship between the GA distribution and hypocotyl cell size by coimaging nlsGPS1 emission ratios with cell margins stained with propidium iodide (PI) (Fig. 6a, Supplementary Fig. 9a). Unlike in rapidly elongating root tips, where larger cells exhibit higher nlsGPS1 emission ratios, we did not detect a correlation between cell size and nlsGPS1 emission ratios in light-grown hypocotyls ($r = -0.09$, Fig. 6a,b). Compared to light-grown hypocotyls, dark-grown hypocotyls exhibited dramatic, GA-dependent cell elongation that can result in a tenfold increase in overall hypocotyl length[42,43]. The rapidly elongating region of dark-grown hypocotyls exhibited larger cells, higher nlsGPS1 emission ratios, and a positive correlation between the two ($r = 0.64$, Fig. 6a,b). Overall, in dark-grown hypocotyls we observed a gradient of nlsGPS1 emission ratios indicative of high GA levels in longer cells transitioning to lower GA levels in the smaller cells of the apical hook (Fig. 6e,f, Supplementary Fig. 10). The emission ratio gradient was not observed in dark-grown hypocotyls of seedlings expressing nlsGPS1-NR or dark-grown hypocotyls of the *ga3ox1, ga3ox2* mutant expressing nlsGPS1 (Fig. 6e,f), suggesting that the gradient of nlsGPS1 emission ratios observed in dark-grown, wild-type hypocotyls is indicative of an actual GA gradient. We also observed pRGA::GFP-RGA protein distribution to be anticorrelated with nlsGPS1 emission ratios in the dark-grown hypocotyls, further supporting the conclusion that nlsGPS1 emission ratios are indicative of GA levels in dark-grown hypocotyls (Supplementary Fig. 4). Combined with the observation of GA accumulation in the root elongation zone (Fig. 3) and stamen filaments (Supplementary Fig. 7), these results indicate that high GA levels correlate with rapid cell elongation in plant development.

Rapid cell elongation in dark-grown hypocotyls depends on both PIF proteins to promote growth[44–46] and elevated GA levels that lead to degradation of growth-repressing DELLA proteins[1]. PIF and GA do not function independently in the hypocotyl as DELLA proteins repress PIF function, and thus elevated GA contributes to PIF-mediated hypocotyl elongation in the dark[47,48]. There is also evidence that light signalling through phytochromes can lower GA levels[17,18], thus reducing hypocotyl elongation by repressing PIF activity both directly, via PIF degradation, and indirectly, via promotion of DELLA accumulation. Compared with wild type, nlsGPS1 emission ratios were modestly increased in light-grown hypocotyls of a *phyA, phyB* mutant (Fig. 6c,d). Because much of phytochrome signalling functions through repression of PIFs, we hypothesized

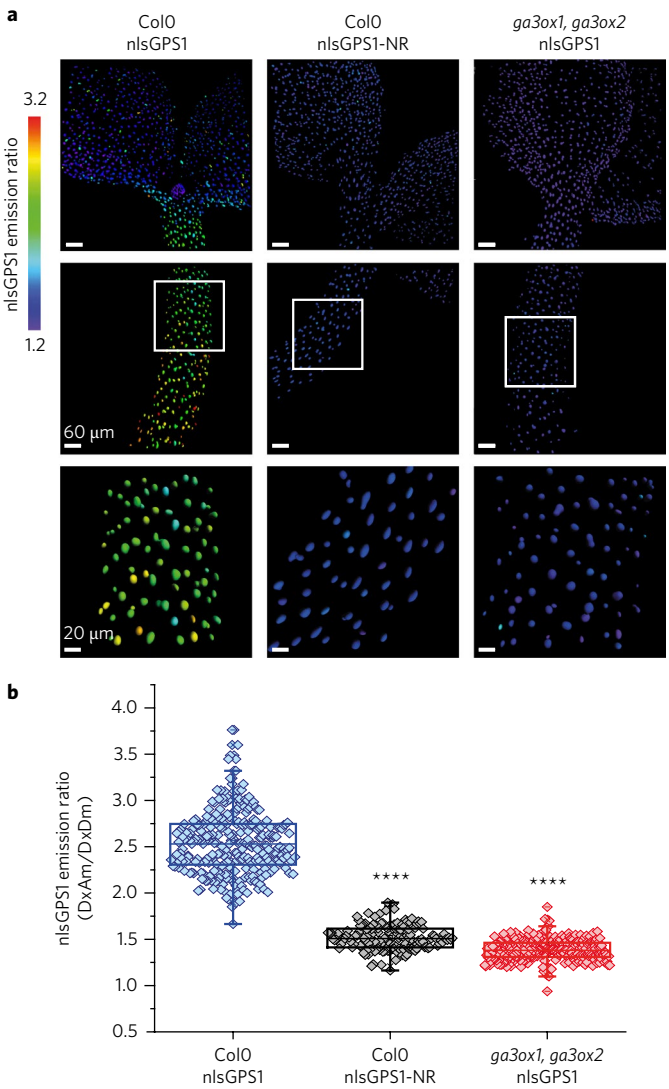

Fig. 5 | Emission ratios of nlsGPS1 in light-grown hypocotyls. a, Three-dimensional images of nlsGPS1 or nlsGPS1-NR emission ratios in hypocotyls 3 days post sowing (upper panels). The central regions of the hypocotyls (250–450 µm from the shoot apical meristem) are shown in the middle panels, with enlarged views in the lower panels. Wild-type Col0 was compared with *ga3ox1, ga3ox2* mutant. Two independent lines of each genotype are also presented in Supplementary Fig. 8. **b**, Beeswarm and box plot of nlsGPS1 emission ratios for nuclei of central region ($n > 261$ nuclei from three independent seedlings for each genotype). nlsGPS1 emission ratios were statistically different in *ga3ox1, ga3ox2* compared to Col0 as were nlsGPS1–NR emission ratios compared to nlsGPS1 (Kruskal-Wallis test ****P value < 0.0001, for nlsGPS1 versus nlsGPS1-NR Cohen's $d = 3.83$, for nlsGPS1 vs *ga3ox1, ga3ox2* mutant Cohen's $d = 4.41$). Complete experiments were repeated at least three times with similar results.

that PIF proteins may regulate the GA gradient in dark-grown hypocotyls, and that the loss of PIFs will lead to reduced GA levels in the light. Correspondingly, nlsGPS1 emission ratios of *pifq* mutant hypocotyls were reduced compared with wild-type hypocotyls grown in the dark (Fig. 6e,f), consistent with PIF proteins being in part responsible for GA elevation in the dark. In the light, where the *pifq* mutant displays no hypocotyl elongation phenotype, we did not observe substantive differences in hypocotyl nlsGPS1 emission ratios between *pifq* and wild type (Supplementary Fig. 11). The finding that PIF proteins elevate GA in hypocotyls in

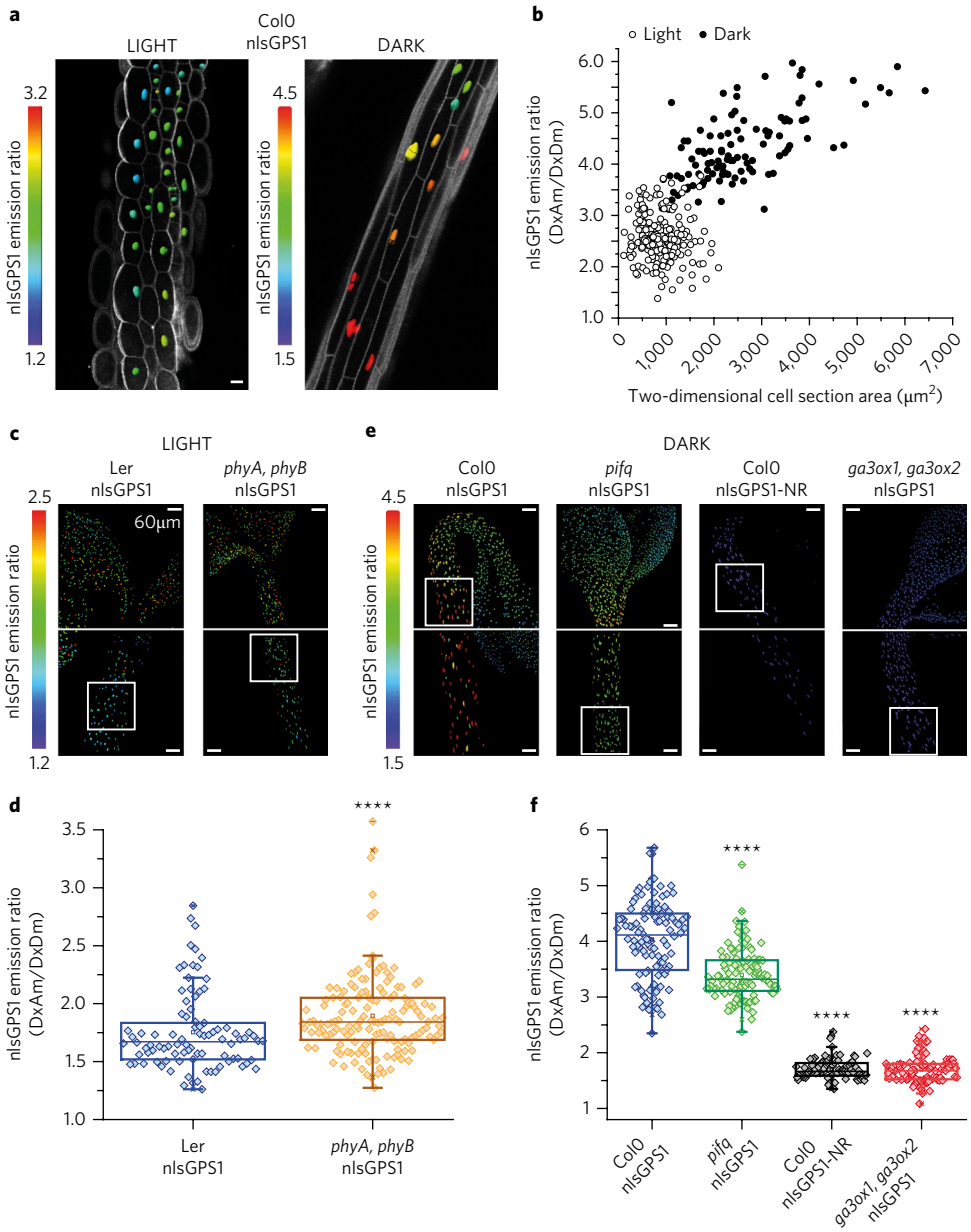

Fig. 6 | Relationship between cell size and nlsGPS1 emission ratio. a, nlsGPS1 emission ratios and PI-labelled cell outlines in light- and dark-grown Col0 hypocotyl epidermal cells. Scale bar = 30 μm. Complete experiments were repeated at least three times with similar results. **b**, Scatter plot showing nlsGPS1 emission ratio and two-dimensional cell section area for individual epidermal cells. For light-grown hypocotyls, correlation coefficient $r = -0.09$; $n = 214$ cells from six hypocotyls. For dark-grown hypocotyls, correlation coefficient $r = 0.64$; $n = 106$ cells from six hypocotyls. **c**, Three-dimensional images of nlsGPS1 or nlsGPS1-NR emission ratios of light-grown hypocotyls 3 days post sowing. Wild-type Ler was compared with *phyA, phyB* mutant. Two independent lines of each genotype are also presented in Supplementary Fig. 10. **d**, Beeswarm and box plot of nlsGPS1 emission ratios for nuclei of central region of hypocotyls, 250–450 μm from shoot apical meristem ($n > 90$ nuclei from three independent seedlings for each genotype); frames demarcating central region are shown. nlsGPS1 emission ratios were statistically different in *phyA, phyB* compared to Ler (Mann-Whitney U test ****P value = 0.0001, Cohen's $d = 0.42$). **e**, Three-dimensional images of dark-grown hypocotyls 3 days post sowing of nlsGPS1 or nlsGPS1-NR. Wild-type Col0 was compared with *ga3ox1, ga3ox2* and *pifq* mutants. Two independent lines of each genotype are also presented in Supplementary Fig. 10. **f**, Beeswarm and box plot of nlsGPS1 emission ratios for nuclei of central region of hypocotyls, 400–600 μm from shoot apical meristem ($n > 100$ nuclei from three independent seedlings for each genotype); example frames indicating the central region are shown in **e**. nlsGPS1 emission ratios were statistically different in *ga3ox1, ga3ox2* and *pifq* compared to Col0 as were nlsGPS1–NR emission ratios compared to nlsGPS1 (Kruskal-Wallis test ****P value < 0.0001, for nlsGPS1 versus *pifq* mutant Cohen's $d = 1.06$, for nlsGPS1 versus nlsGPS1 Cohen's $d = 4.48$, for nlsGPS1 versus *ga3ox1, ga3ox2* mutant Cohen's $d = 4.40$). Complete experiments were repeated at least three times with similar results.

the dark is supported by RNA sequencing (RNA-Seq) experiments indicating that PIFs positively regulate expression of the GA biosynthetic enzyme *AtGA20ox3* in dark-grown seedlings[49]. Interestingly, the elevation of nlsGPS1 emission ratios below the apical hook of etiolated hypocotyls is reduced in the *pifq* mutant, indicating a potential role for the PIFs in controlling cellular GA distribution in hypocotyls (Fig. 6e,f). As GA accumulation promotes PIF activity through stimulating degradation of the PIF-repressing DELLA

proteins, our findings support a hypocotyl growth model with a PIF positive feedback loop through GA signalling.

Discussion

Plant hormones are mobile, small signalling molecules that play central roles in plant development and environmental responses. The goal of a systems level understanding of the upstream regulation and downstream consequences of hormone accumulations and depletions demands a more accurate and higher resolution quantification of dynamic hormone patterning. Unlike other quantification methods, fluorescent biosensors that directly report on plant hormones are minimally invasive, high-resolution and require only light inputs once the biosensor is expressed from the host cell genome[26]. Compared with transcriptional reporters and signalling sensors, hormone quantification using direct biosensors is also less susceptible to non-linear signalling responses, variations in signalling components independent of the hormone and crosstalk from other signalling pathways[50]. Here we report the engineering and analysis of the first such biosensor for GA, a key signalling molecule that affects plant morphogenesis.

Engineering of a biosensor for GA. The GA biosensor GPS1 was developed and optimized using a combinatorial FRET biosensor engineering platform developed previously[24]. GPS1 reports GA levels via a ratiometric, fluorescent output (Fig. 1). GPS1 is a single synthetic polypeptide composed of an output domain based on improved variants of cyan fluorescent protein and yellow fluorescent protein fused with a sensory domain based on the GID1C–GAI receptor complex from *Arabidopsis* (Fig. 1b). GPS1 directly interacts with GA_4 with high affinity (in vitro apparent K_d for $GA_4 = 24$ nM) and other bioactive GAs with lower affinity (Fig. 2a). Although GA_4 is considered to be the dominant bioactive GA in *Arabidopsis*, GPS1 could also report on other GAs in vivo if present at appreciable concentrations (for example, around the K_d of 110 nM for GA_1). In the future, GPS biosensors could potentially be re-engineered to have altered selectivity and affinity for the various GAs. The high-affinity association of GPS1 with GA_4 is apparently not rapidly reversible (Fig. 2c), and thus GPS1 emission ratios likely report the highest recent GA concentration reached in the solution or cellular compartment harbouring the biosensor. Thus, GPS1 will probably not report decreasing GA levels. Nevertheless, the ability to deploy the GPS1 fusion protein in living cells permits minimally invasive GA biosensing with unprecedented spatiotemporal resolution.

GA gradients in vivo. The GPS1 biosensor was targeted to the nucleus (nlsGPS1) in transgenic *Arabidopsis* plants to investigate the GA distribution in nuclei elongating root and shoot tissues and the quantitative relationship between GA accumulation and cell elongation. It has been proposed that GA levels in root tip cells are inversely correlated with cell length, that is, to be high in the root division zone and to be depleted due to cytosolic dilution as cells elongate[9]. Rather than an inverse relationship, we found GA—as indicated by GPS1 emission ratios—to be positively correlated with cell length (Figs. 3 and 4). In another tissue where pronounced cell elongation requires GA, the dark-grown hypocotyl, we again observed GA to be correlated with cell length (Fig. 6). These correlations are compatible with a hypothesis that GA induces cell growth locally in a dose-dependent manner. Thus, the patterning of GA enzymatic and transport activities that set GA levels would influence the patterning of cell elongation. We show that the pattern of accumulation of exogenous GA_4 in roots closely mirrors the distribution of endogenous GA, indicating that differential accumulation of GA from other cells or tissues could generate a GA gradient, and thus a gradient of cell length, in the root elongation zone (Fig. 4). Understanding the signalling pathways that regulate these activities, whether via patterning GA enzyme activity, transport activity or both, is key to understanding how GA distribution links environmental stimuli and endogenous factors to their downstream effects on plant growth and development.

Factors affecting GA gradients. Because light signalling is known to impact expression of GA enzymes in monocots and dicots, including *Arabidopsis*[16–18], we investigated the regulation of the GA distribution by light. In the light, activation of phytochromes, such as PhyA and PhyB, contributes to a reduction in hypocotyl cell length compared to hypocotyls grown in the dark[29]. Compared with wild type, light-grown hypocotyls of a *phyA, phyB* mutant[29] exhibited elevated GA, confirming a role for light signalling through phytochromes in lowering GA levels alongside hypocotyl cell length (Fig. 6). However, it remained unknown what factors promote GA elevation in dark-grown hypocotyls and how phytochrome signalling lowers GA levels in the light. We provide genetic evidence that the PIFs fulfil, at least in part, both roles in affecting GA levels (Fig. 6). As GA signalling influences hypocotyl elongation largely through promoting PIF activity[47,48], PIF promotion of GA accumulation represents a positive feedback loop within the molecular framework driving rapid hypocotyl growth. Furthermore, positive regulation of GA by PIFs in the hypocotyl stands in marked contrast to repression of GA by PIF1 activity in seeds[19], and represents a new link between light signalling and hormone distribution that underpins cellular growth and developmental plasticity. However, because we observed only a modest increase in GA levels in *phyA, phyB* mutant hypocotyls in the light and partial reduction in GA levels in *pifq* mutant hypocotyls in the dark (Fig. 6), it is likely that other phytochromes and other light signalling components beyond the phytochromes and the PIFs regulate GA in hypocotyls. Indeed, during photomorphogenesis, both phytochromes and cryptochromes affect GA biosynthetic and catabolic enzymes[18].

Because myriad other signals have been shown to regulate GA levels[1], and because local GA elevation may define regions of rapid cell elongation (Figs. 3 and 6), it is likely that a finely tuned ensemble of GA enzymatic and transport steps in concert with their regulators together determine GA distribution dynamics in vivo. A precise understanding of how GA distribution is controlled and how it, in turn, contributes to patterning plant cell growth warrants further investigation. Such an understanding could lead to strategic interventions into GA distributions in crop plants for specific improvements in germination, flowering-time, plant architecture, organ size and environmental responses.

Methods

Gateway entry clone and destination vector libraries. Potential GA binding domains to be incorporated in a screen for FRET GA biosensors were designed as combinations of an AtGID1 GA receptor protein linked to a truncation of a DELLA protein and cloned as a Gateway Entry Clone library. The specific components were full-length AtGID1A (AT3G05120), AtGID1B (AT3G63010) and AtGID1C (AT5G27320), truncated AtGAI D28 – D101 and G26 – L91 (At1g14920), truncated AtRGA D44 – N117 and N41 – N108 (At2g01570) and five internal linkers described previously (L12, L52, L65, L71, L118[24]). Potential GA binding domains were amplified in two PCR steps. In the first step, N-terminal domain sequences were amplified with 5' primers containing the attB1 site and 3' primers containing a 30-base pair sequence for overlapping PCR. C-terminal domain sequences were amplified with 5' primers containing the same 30-base pair sequence for overlapping PCR and 3' primers containing the attB2 site. In the second step, two products from the first reactions were amplified together in an overlap extension PCR reaction, and the resulting product was recombined into pDONR221 in a Gateway BP recombination reaction resulting in a potential GA binding domain Entry Clone. The 30-base pair overlap sequence codes for a flexible L12 and contains *Asc*I and *Fse*I restriction sites for subsequent insertion of additional linker sequences. Primers for amplification are listed in Supplementary Table 1. In the second round of screening, the selected GA binding domain Entry Clones were digested with *Asc*I and *Fse*I (NEB) for insertion of one of four additional linker sequences as described previously[24]. The pDR FLIP Destination vectors for expression of biosensors in yeast were described previously[24] and are available from AddGene (https://www.addgene.org/Wolf_Frommer/).

Generation of GPS1-NR mutants. The GA binding domain Entry Clone for GPS1 was altered using QuikChange (Agilent) site-directed mutagenesis according to manufacturer's instructions to generate the GPS1-NR mutations. Primers for site-directed mutagenesis of GPS1 to create GPS1-NR are included in Supplementary Table 1.

Expression of sensors in protease deficient yeast. pDR FLIP Destination vectors were recombined in Gateway LR reactions with GA binding domain Entry Clones resulting in yeast expression plasmids coding for various biosensor designs. *Saccharomyces cerevisiae* strain BJ5465 (ATCC 208289 (*MATa ura3-52 trp1 leu2-Δ 1 his3-Δ200 pep4::HIS3 prb1-Δ1.6 R can1 GAL*)[30]) was transformed with yeast expression plasmids in 96-well format using a lithium acetate transformation protocol[51]. Transformed yeasts were plated on synthetic complete (SC) medium with 0.8 % agar (BD) supplemented with 240 mg l^{-1} leucine and 20 mg l^{-1} tryptophan (SC agar +Leu,Trp) to select for complementation of uracil auxotrophy by the URA3 marker of the pDR FLIP-based expression clones. Transformants were grown in 2 × 1 ml cultures in SC medium +Leu,Trp in 96-well culture blocks (Greiner) for preliminary fluorescence analysis of sensor expression and for high-throughput screening of sensors in cleared cell lysates. For metal-affinity chromatography purification of sensors, yeast strains expressing sensors were grown in 30 ml cultures in SC medium +Leu,Trp in 50 ml culture tubes.

Fluorescence analysis of cell lysates. Yeast cell cultures (A_{600} ~1.0) were centrifuged at 5000 g for 7 minutes, washed once in 1 mL PBS buffer (137 mM NaCl, 2.7 mM KCl, 10 mM Na_2HPO_4, 1.8 mM KH_2PO_4, pH 7.4), transferred to a 96-well culture block (in the case of 30 mL cultures) and centrifuged a second time at 5,000 g for 7 minutes. The cell pellets were then frozen at −80 °C. Frozen cell pellets were resuspended in 1 ml PBS buffer. A 50 µl aliquot was transferred to a clear bottom microtiter plate (Greiner) for analysis of whole cell fluorescence. Cells were then centrifuged at 5,000 g for 7 minutes before 700 µl chilled glass bead slurry (PBS buffer, 0.1% Triton X-100 and 50% (v/v) Zirconia/Silica beads (0.5 mm; BioSpec)) was added to each cell pellet. The culture block was then sealed with aluminium foil tape (3 M 439 Silver, 3-1/4 in width) and vortexed until pellets were resuspended. The block was then loaded into a Retsch MM300 mixer mill, which was run for 15 minutes at a frequency setting of 20. Cell lysate was centrifuged at 5000 g for 10 min at 4 °C, after which 200 µl of supernatant was transferred to a microtiter plate and centrifuged again (5,000 g for 5 min) to remove remaining cell debris. The resulting supernatant was then diluted in PBS buffer for use in fluorescence analysis in clear bottom microtiter plates using a fluorometer (Tecan). Samples were diluted in 20 mM MOPS pH 7.4 in order to obtain fluorescence emission at 480 nm and 530 nm between 5,000 and 50,000 relative fluorescence units with an excitation wavelength of 428 nm and a gain between 70 and 100. For all imaging, bandwidth was set to 12 nm, number of flashes was ten and integration time was 40 µs. Fluorescence readings were acquired for donor fluorophore (excitation 428 nm, emission 485 nm), acceptor fluorophore (excitation 500 nm, eYFP emission 535 nm) and for energy transfer from donor to acceptor (excitation 428 nm, emission 530 nm). Additionally, a fluorescence emission scan reading from 470 to 550 nm (step size 5 nm) with an excitation wavelength of 428 nm was acquired. Cell lysates from BJ5465 yeast containing an empty vector were used as a negative control for background subtraction.

To analyse sensor response to GA, 100 µl of each sensor sample were combined with 50 µl 10 µM GA_3 in water (diluted from 10 mM GA_3 in 100% ethanol stock solution) or a mock treatment lacking GA. Replicates were averaged, and a ratio of DxAm/DxDm was calculated as an approximation of FRET ratio. GA-dependent ratio change was calculated as the DxAm/DxDm with GA over DxAm/DxDm mock.

Fluorescence analysis of purified sensors. For purification of the biosensors by metal affinity chromatography, yeast lysates were diluted 1:2 in 20 mM TRIS-HCl, 5 mM imidazole, pH 7.4 and then filtered through a 0.45 µm polyethersulfone (PES) filter and bound to Poly-Prep chromatography columns (Bio-Rad) containing His-bind resin (Novagen). Columns were then washed twice with 20 mM Tris-HCl, 5 mM imidazole, pH 7.4 and eluted in 20 mM TRIS-HCl, 200 mM imidazole, pH 7.4. Alternatively, lysates were diluted 1:2 in 50 mM MOPS, 10 mM imidazole, pH 7.4 and then filtered through a 0.45 µm PES filter and bound to Poly-Prep chromatography columns (Bio-Rad) containing His-Pur Cobalt resin (Pierce). Columns were then washed twice with 50 mM MOPS, 10 mM imidazole, pH 7.4 and eluted in 50 mM MOPS, 150 mM imidazole, pH 7.4. In all cases, samples were diluted in 50 mM MOPS pH 7.4 and fluorescence was analysed on a Safire fluorometer (Tecan) as described for cleared cell lysates or a SpectraMax fluorometer (Molecular Biosciences). Determination of the apparent K_d of GPS1 for various GAs was performed as described previously[52]. All chemicals were from Sigma with the exception of the GAs, which were from OlChemIm. Data are reported as means and s.d.'s of 3–4 replicates, and each experiment was performed at least three times with similar results. The reversibility of binding of GAs by GPS1 protein was tested using Zeba Spin Desalting Columns, 0.5 ml, 40 K MWCO (Thermo Scientific). The purified GPS1 protein was pretreated with 0 µM GA, 0.1 µM GA_4, 1 µM GA_3 or 1 µM GA_1. After two 20 minute buffer exchange steps with 50 mM MOPS pH 7.4 using Zeba Spin columns according to manufacturer's instructions, the eluted GPS1 in 50 mM MOPS pH 7.4 was treated with 0 µM GA and 0.1 µM GA_4 and fluorescence was analysed on a SpectraMax fluorometer. The donor fluorophore was excited at a wavelength of 430 nm and the fluorescence emission scan from 460 to 560 nm (step size 5 nm) was acquired. The emission ratio was subsequently calculated dividing the mean value across the 530–535 nm range by that across the 480–485 nm range.

Expression of GPS1 in planta. The p16 promoter[33] from the AT3G60245 gene encoding a 16 S ribosomal subunit was used to drive the nuclear-localized GPS1 fusion biosensor in plants. The following construct was inserted into the multiple cloning site of the p16-Kan vector[33]: 5′ – a sequence coding for the SV40 derived nuclear localization signal LQPKKKRKVGG[53]; a sequence coding for the enhanced dimer variant of Aphrodite with a nine-amino acid C-terminal truncation (edAFPt9); a Gateway cassette including attR1, Chloramphenicol resistance gene, ccdB terminator gene and attR2; a sequence coding for the enhanced dimer variant of Cerulean (edCer); and a sequence coding for the cMyc epitope tag – 3'. The resulting Gateway Destination vector (p16-FLIPnls43) was then recombined in Gateway LR reactions with GA binding domain Entry Clones resulting in GPS1 and GPS1–NR expression clones. The map and sequence of p16-nlsGPS1 and p16-nlsGPS1-NR are included in Supplementary File 1.

Transgenic plant lines expressing GPS1. Transgenic plant lines were generated using the *Agrobacterium* floral dip method as described previously[22]. Transformants were selected on agar plates containing ½ × Murashige Skoog (MS) medium with Kanamycin. Fluorescence expression of transformants on agar plates was analysed using a FluorChem Q imager (Alpha Innotech) with CY2 excitation and emission and the following settings: 12 second exposure time, normal speed, ultra-resolution and level 2 noise reduction. All GPS1 plant lines are described in Supplementary Table 1, including GPS1 lines in the following mutant backgrounds sourced from ABRC (CS6224 – *phyA, phyB*, CS66049 – *pif1, pif3, pif4, pif5*, CS6944 – *ga3ox1, ga3ox2*). pRGA::GFP-RGA in Col0 (NASC ID – N16360) is described here[35].

Phenotypic characterization of plant lines expressing GPS1. For hypocotyl and root length assays, plant lines were grown vertically on ½ × MS agar medium (½ × MS salts (PhytoTechnology Lab), 0.8 % Agar (BD), 0.05% (w/v) MES pH 5.7). Plates were stratified for 2 days at 4 °C, after which they were exposed to 30 h of light and then transferred to a dark-growth chamber (24 h dark, 22 °C, 70% relative humidity (RH)). For experiments, 10 mM GA_4 (Olchemim) and 10 mM Paclobutazol (PBZ, Sigma-Aldrich) stock solutions were prepared in 70% ethanol. Germinated seeds were transferred to ½ × MS agar medium supplied with PBZ (0 µM, 1 µM and 10 µM) and GA_4 (0 µM, 0.01 µM and 10 µM). Plates were imaged after 5 days, and hypocotyl and root lengths were measured using FIJI (http://fiji.sc/). Each experiment included ~15 seedlings per genotype and was repeated three independent times with similar results. Homozygous biosensor expressing lines were compared with isogenic wild-type lines segregated from heterozygous T1 parents.

Seedling growth, RootChip16 device preparation and root perfusion. The RootChip16 device was used as described in detail previously[23,54]. Briefly, the device was sterilized by ultraviolet light exposure and immersed in liquid growth media (¼ × MS salts, 0.025% (w/v) MES pH 5.7 supplemented with B vitamins at final concentrations of niacin 2.3 µM, thiamine 1.5 µM, pyridoxin 1.2 µM and myo-inositol 0.3 µM (Sigma)) for removal of air in the root observation chambers by application of suction at the solution outlets using a microliter pipette. *Arabidopsis* seedlings had been germinated on 5-mm-long portions of 10 µl pipette tips filled with solidified growth medium (½ × MS salts, 1% Agar, 0.05% (w/v) MES pH 5.7 supplemented with B vitamins at final concentrations of niacin 4.6 µM, thiamine 3.0 µM, pyridoxin 2.4 µM and myo-inositol 0.6 µM). At 5 days, the seedlings were placed onto the chip by plugging the tips into the root inlets. The chip was incubated for 24 h under standard long-day growth conditions (16 h light/8 h dark cycling, 22 °C, 70% RH) to allow roots to grow into the observation chambers. Before imaging, the RootChip16 was inserted from below into the central aperture of the carrier and fixed with tape and pressure lines, for control over micromechanical valves, and connected to solution lines. To actuate the push-up valves on the chip, a closing pressure of 15 p.s.i. (1.03 bar) was applied to the water-filled control lines. Solution vials were pressurized with 5–10 p.s.i. (0.34 bar) to drive perfusion solutions through the flow lines of the device.

In planta analysis of GPS1 using the RootChip16. The RootChip16 was constantly perfused with ¼ × MS medium (¼ × MS salts, 0.025% MES pH 5.7). For experiments, 10 mM GA_4 stock solutions were prepared in 100% ethanol and diluted in ¼ × MS medium. Vials with solutions were connected to root chip flow lines and pressurized. Perfusion of solutions was controlled by the RootChip16 control valves[23,54] connected to a valve controller controlled by a LabView (National Instruments) program.

Fluorescence microscopy. *Arabidopsis* plants were grown vertically on ½ × MS agar medium (½ × MS salts, 0.8 % Agar, 0.05% MES pH 5.7) plates. Plates were

stratified for 2 days at +4 °C in the dark prior to being placed in a growth chamber with long-day growth conditions (16 h light/8 h dark cycling, temperature cycling 22 °C day/18 °C night, 70% RH) or darkness (accomplished by wrapping agar plates in foil) for the indicated number of days post sowing. Dark-grown seedlings were additionally exposed to 3–6 hours of light before wrapping in foil. *ga3ox1, ga3ox2* mutant seedlings were additionally treated with 1 µM GA_4 during stratification followed by washing with water and plating. All light-grown seedling experiments were initiated between 4–10 hours after the onset of the light period. Seedlings were placed in solution containing ¼ × MS medium (¼ × MS salts, 0.025% MES pH 5.7) and prepared for imaging on either glass slides or the RootChip16. For GA and cycloheximide treatments on glass slides, seedlings were placed on glass slides with 50 µL solution and surrounded with a rectangle of vacuum grease and covered with a square cover slip equal in height and half the width of the vacuum grease rectangle. The GA treatment solution could then be exchanged beneath the coverslip by addition to the left and removal from the right side of the coverslip. Images were acquired before and 20 minutes after exchange of the solution around the seedlings.

Confocal images were acquired on a Leica SP8-FLIMan using a ×20 dry 0.70 HC PLAN APO objective. To excite cyan fluorescent protein (CFP) and YFP, 448 nm and 514 nm lasers were used, respectively. The 552 nm laser line was used to excite PI. The 448 nm laser line was set to 10% for green fluorescent protein (GFP) excitation. For root imaging with PI (10 mgl^{-1} working solution), a × 25 0.95 NA water objective was used. Fluorescence emission was detected by HyD SMD detectors, set to detect 460 to 500 nm for CFP, 525 to 560 nm for YFP, 590 to 635 nm for PI and 500 to 535 nm for GFP. The laser power was set between 0.5% and 2% with detector gain set to 110 to image CFP or YFP. A line average of four was used for the majority of experiments, except for imaging nlsGPS1-NR, where a line average of eight was used to improve the signal-to-noise ratio. The *z*-stacks were acquired with a step-size of 1–2 µm depending upon the experiment.

RootChip imaging was performed using a × 20 0.70 HC PL APO objective on an inverted spinning disk confocal; 442 nm and 514 nm lasers were used for excitation of CFP and YFP, respectively. Emission filters were 458–482 nm for CFP and 520–550 nm for YFP. Fluorescence emission was detected by an Andor iXon camera. A typical acquisition used an intensification setting of 300, a gain setting of two, a 400 ms exposure for DxDm and DxAm or 100 ms exposure for AxAm, a Z-stack of three 5 µm steps and imaging intervals of 5 minutes.

Image processing and analysis. For confocal images acquired on glass slides, image processing and analysis were performed by using IMARIS 8.3.1 (Bitplane). Surfaces were segmented based on YFP channel using the 'surfaces wizard' and the following settings: background subtraction (local contrast) set to 3 µm, thresholding set as default. For the cycloheximide assay and pRGA::GFP-RGA distribution, surfaces were false-coloured according to the mean of the masked YFP or GFP channel, respectively. The ratio channel (DxAm/DxDm) was calculated by using the IMARIS Xtension 'XT *Mean Intensity Ratio*', which computes a ratio between existing mean intensity statistics in IMARIS using Matlab. The extension computes and stores the ratio of the intensity means of individual surfaces in the provided channels. For Root-Chip experiments, the ratio channel (DxAm/DxDm) was calculated by using the Matlab extension '*Channel Arithmetics*'.

For confocal images acquired using the RootChip16, image processing and analysis were performed using deprecated three-dimensional stitching (FIJI Macro by Stephan Preibisch, http://fly.mpi-cbg.de/~preibisch/contact.html) of the four root positions followed by four-dimensional analysis using IMARIS 8.3.1 (BitPlane).

In this work, we presented data using beeswarm and box plot of raw data. In the beeswarm and box plot graphs, the central rectangle spans the first quartile to the third quartile, while the line inside the rectangle shows the median. The whiskers denote 1.5 interquartile ranges from the box and outlying values plotted beyond the whiskers. All the statistical analyses were performed using OriginPro (http://www.originlab.com/Origin).

Data availability. The datasets generated during and/or analysed during the current study are available from the corresponding authors on reasonable request. Seed stocks have been deposited with the Nottingham Arabidopsis Stock Centre with the IDs N2107734–N2107739. Plasmids have been deposited with Addgene with the IDs 101081–101085.

Received: 17 February 2017; Accepted: 24 August 2017;
Published online: 02 October 2017

References

1. Sun, T. P. Gibberellin metabolism, perception and signaling pathways in *Arabidopsis*. *Arabidopsis Book* **6**, e0103 (2008).
2. Stowe, B. B. & Yamaki, T. The history and physiology of the gibberellins. *Annu. Rev. Plant Physiol.* **1957**, 181–216 (1957).
3. Hu, J. et al. Potential sites of bioactive gibberellin production during reproductive growth in *Arabidopsis*. *Plant Cell* **20**, 320–336 (2008).
4. Mitchum, M. G. et al. Distinct and overlapping roles of two gibberellin 3-oxidases in *Arabidopsis* development. *Plant J.* **45**, 804–818 (2006).
5. Plackett, A. R. et al. Analysis of the developmental roles of the *Arabidopsis* gibberellin 20-oxidases demonstrates that GA20ox1, -2, and -3 are the dominant paralogs. *Plant Cell* **24**, 941–960 (2012).
6. Sun, N. et al. *Arabidopsis* SAURs are critical for differential light regulation of the development of various organs. *Proc. Natl Acad. Sci. USA* **113**, 6071–6076 (2016).
7. Okamoto, M. et al. Measurement of abscisic acid and gibberellins by gas chromatography/mass spectrometry. *Methods Mol. Biol.* **495**, 53–60 (2009).
8. Achard, P. et al. Gibberellin signaling controls cell proliferation rate in *Arabidopsis*. *Curr. Biol.* **19**, 1188–1193 (2009).
9. Band, L. R. et al. Growth-induced hormone dilution can explain the dynamics of plant root cell elongation. *Proc. Natl Acad. Sci. USA* **109**, 7577–7582 (2012).
10. Bassel, G. W. et al. Mechanical constraints imposed by 3D cellular geometry and arrangement modulate growth patterns in the *Arabidopsis* embryo. *Proc. Natl Acad. Sci. USA* **111**, 8685–8690 (2014).
11. Ubeda-Tomas, S. et al. Root growth in *Arabidopsis* requires gibberellin/DELLA signalling in the endodermis. *Nat. Cell Biol.* **10**, 625–628 (2008).
12. Ubeda-Tomas, S. et al. Gibberellin signaling in the endodermis controls *Arabidopsis* root meristem size. *Curr. Biol.* **19**, 1194–1199 (2009).
13. Shani, E. et al. Gibberellins accumulate in the elongating endodermal cells of *Arabidopsis* root. *Proc. Natl Acad. Sci. USA* **110**, 4834–4839 (2013).
14. Bentsink, L. & Koornneef, M. Seed dormancy and germination. *Arabidopsis Book* **6**, e0119 (2008).
15. Jiang, Z. et al. Phytochrome B and REVEILLE1/2-mediated signalling controls seed dormancy and germination in *Arabidopsis*. *Nat. Commun.* **7**, 12377 (2016).
16. Hirose, F. et al. Cryptochrome and phytochrome cooperatively but independently reduce active gibberellin content in rice seedlings under light irradiation. *Plant Cell Physiol.* **53**, 1570–1582 (2012).
17. Reid, J. B. et al. Control of gibberellin levels and gene expression during de-etiolation in pea. *Plant Physiol.* **128**, 734–741 (2002).
18. Zhao, X. et al. A study of gibberellin homeostasis and cryptochrome-mediated blue light inhibition of hypocotyl elongation. *Plant Physiol.* **145**, 106–118 (2007).
19. Oh, E. et al. Light activates the degradation of PIL5 protein to promote seed germination through gibberellin in *Arabidopsis*. *Plant J.* **47**, 124–139 (2006).
20. Ast, C. et al. Ratiometric Matryoshka biosensors from a nested cassette of green- and orange-emitting fluorescent proteins. *Nat. Commun.* **8**, 431 (2017).
21. Monshausen, G. B., Messerli, M. A. & Gilroy, S. Imaging of the Yellow Cameleon 3.6 indicator reveals that elevations in cytosolic Ca2+ follow oscillating increases in growth in root hairs of *Arabidopsis*. *Plant Physiol.* **147**, 1690–1698 (2008).
22. Deuschle, K. et al. Rapid metabolism of glucose detected with FRET glucose nanosensors in epidermal cells and intact roots of *Arabidopsis* RNA-silencing mutants. *Plant Cell* **18**, 2314–2325 (2006).
23. Grossmann, G. et al. The RootChip: an integrated microfluidic chip for plant science. *Plant Cell* **23**, 4234–4240 (2011).
24. Jones, A. M. et al. Abscisic acid dynamics in roots detected with genetically encoded FRET sensors. *eLife* **3**, e01741 (2014).
25. Waadt, R. et al. FRET-based reporters for the direct visualization of abscisic acid concentration changes and distribution in *Arabidopsis*. *eLife* **3**, e01739 (2014).
26. Okumoto, S., Jones, A. & Frommer, W. B. Quantitative imaging with fluorescent biosensors. *Annu. Rev. Plant Biol.* **63**, 663–706 (2012).
27. Ueguchi-Tanaka, M. et al. Molecular interactions of a soluble gibberellin receptor, GID1, with a rice DELLA protein, SLR1, and gibberellin. *Plant Cell* **19**, 2140–2155 (2007).
28. Sun, T. P. Gibberellin-GID1-DELLA: a pivotal regulatory module for plant growth and development. *Plant Physiol.* **154**, 567–570 (2010).
29. Reed, J. W. et al. Phytochrome A and Phytochrome B have overlapping but distinct functions in *Arabidopsis* development. *Plant Physiol.* **104**, 1139–1149 (1994).
30. Jones, E. W. Tackling the protease problem in *Saccharomyces cerevisiae*. *Methods Enzymol.* **194**, 428–453 (1991).
31. Murase, K. et al. Gibberellin-induced DELLA recognition by the gibberellin receptor GID1. *Nature* **456**, 459–463 (2008).
32. Nakajima, M. et al. Identification and characterization of *Arabidopsis* gibberellin receptors. *Plant J.* **46**, 880–889 (2006).
33. Schuster, C. et al. A regulatory framework for shoot stem cell control integrating metabolic, transcriptional, and phytohormone signals. *Dev. Cell* **28**, 438–449 (2014).
34. Palmer, A. E. et al. Ca2+ indicators based on computationally redesigned calmodulin-peptide pairs. *Chem. Biol.* **13**, 521–530 (2006).
35. Silverstone, A. L. et al. Repressing a repressor: gibberellin-induced rapid reduction of the RGA protein in *Arabidopsis*. *Plant Cell* **13**, 1555–1566 (2001).

36. Kato, J. Nonpolar transport of gibberellin through pea stem and a method for its determination. *Science* **128**, 1008–1009 (1958).
37. Dayan, J. et al. Leaf-induced gibberellin signaling is essential for internode elongation, cambial activity, and fiber differentiation in tobacco stems. *Plant Cell* **24**, 66–79 (2012).
38. Eriksson, S. et al. GA4 is the active gibberellin in the regulation of LEAFY transcription and *Arabidopsis* floral initiation. *Plant Cell* **18**, 2172–2181 (2006).
39. King, R. W. et al. Long-day induction of flowering in *Lolium temulentum* involves sequential increases in specific gibberellins at the shoot apex. *Plant Physiol.* **127**, 624–632 (2001).
40. Ragni, L. et al. Mobile gibberellin directly stimulates *Arabidopsis* hypocotyl xylem expansion. *Plant Cell* **23**, 1322–1336 (2011).
41. Cheng, H. et al. Gibberellin regulates *Arabidopsis* floral development via suppression of DELLA protein function. *Development* **131**, 1055–1064 (2004).
42. Cowling, R. J. & Harberd, N. P. Gibberellins control *Arabidopsis* hypocotyl growth via regulation of cellular elongation. *J. Exp. Bot.* **50**, 1351–1357 (1999).
43. Gendreau, E. et al. Cellular basis of hypocotyl growth in *Arabidopsis thaliana*. *Plant Physiol.* **114**, 295–305 (1997).
44. Leivar, P. et al. The *Arabidopsis* phytochrome-interacting factor PIF7, together with PIF3 and PIF4, regulates responses to prolonged red light by modulating phyB levels. *Plant Cell* **20**, 337–352 (2008).
45. Shin, J. et al. Phytochromes promote seedling light responses by inhibiting four negatively-acting phytochrome-interacting factors. *Proc. Natl Acad. Sci. USA* **106**, 7660–7665 (2009).
46. Castillon, A., Shen, H. & Huq, E. Phytochrome Interacting Factors: central players in phytochrome-mediated light signaling networks. *Trends Plant Sci.* **12**, 514–521 (2007).
47. de Lucas, M. et al. A molecular framework for light and gibberellin control of cell elongation. *Nature* **451**, 480–484 (2008).
48. Feng, S. et al. Coordinated regulation of *Arabidopsis thaliana* development by light and gibberellins. *Nature* **451**, 475–479 (2008).
49. Zhang, Y. et al. A quartet of PIF bHLH factors provides a transcriptionally centered signaling hub that regulates seedling morphogenesis through differential expression-patterning of shared target genes in *Arabidopsis*. *PLoS Genet.* **9**, e1003244 (2013).
50. Jones, A. M. et al. In vivo biochemistry: applications for small molecule biosensors in plant biology. *Curr. Opin. Plant Biol.* **16**, 389–395 (2013).
51. De Michele, R. et al. Fluorescent sensors reporting the activity of ammonium transceptors in live cells. *eLife* **2**, e00800 (2013).
52. Deuschle, K. et al. Genetically encoded sensors for metabolites. *Cytometry A* **64**, 3–9 (2005).
53. Kalderon, D. et al. A short amino acid sequence able to specify nuclear location. *Cell* **39**, 499–509 (1984). (3 Pt 2).
54. Grossmann, G. et al. Time-lapse fluorescence imaging of *Arabidopsis* root growth with rapid manipulation of the root environment using the RootChip. *J Vis. Exp.* **65**, e4290 (2012).
55. Rekas, A. et al. Crystal structure of venus, a yellow fluorescent protein with improved maturation and reduced environmental sensitivity. *J. Biol. Chem.* **277**, 50573–50578 (2002).
56. Lelimousin, M. et al. Intrinsic dynamics in ECFP and Cerulean control fluorescence quantum yield. *Biochemistry* **48**, 10038–10046 (2009).

Acknowledgements

We gratefully acknowledge S. Manoj-Kumar for technical assistance and B. DeMeo for development of XT Mean Intensity Ratio. We thank the Gatsby Charitable Foundation for funding support of A.R., A.W. and A.M.J.

Author contributions

A.R., A.W., V.L. and A.M.J. ran the experiments. A.R., A.W., V.L. and A.M.J. analysed the results. A.R. and A.M.J. wrote the manuscript, and W.B.F. and A.M.J. designed and supervised the project.

Competing interests

The authors declare no competing financial interests.

Additional information

Supplementary information is available for this paper at https://doi.org/10.1038/s41477-017-0021-9.

Reprints and permissions information is available at www.nature.com/reprints.

Correspondence and requests for materials should be addressed to W.B.F. or A.M.J.

Publisher's note: Springer Nature remains neutral with regard to jurisdictional claims in published maps and institutional affiliations.

nature research

Corresponding author(s): Alexander M. Jones

☐ Initial submission ☐ Revised version ☒ Final submission

Life Sciences Reporting Summary

Nature Research wishes to improve the reproducibility of the work that we publish. This form is intended for publication with all accepted life science papers and provides structure for consistency and transparency in reporting. Every life science submission will use this form; some list items might not apply to an individual manuscript, but all fields must be completed for clarity.

For further information on the points included in this form, see Reporting Life Sciences Research. For further information on Nature Research policies, including our data availability policy, see Authors & Referees and the Editorial Policy Checklist.

Experimental design

1. Sample size

Describe how sample size was determined.

We have chosen our sample size to ensure adequate power. This is based on our pilot and exploratory experiments.

2. Data exclusions

Describe any data exclusions.

We did not exclude any plant from our analysis.

3. Replication

Describe whether the experimental findings were reliably reproduced.

Complete experiments were repeated at least three times with similar results.

4. Randomization

Describe how samples/organisms/participants were allocated into experimental groups.

Our samples/ plants were random.

5. Blinding

Describe whether the investigators were blinded to group allocation during data collection and/or analysis.

Investigators were not blinded to group allocation during data collection and/or analysis.

Note: all studies involving animals and/or human research participants must disclose whether blinding and randomization were used.

6. Statistical parameters

For all figures and tables that use statistical methods, confirm that the following items are present in relevant figure legends (or in the Methods section if additional space is needed).

n/a	Confirmed	
☐	☒	The exact sample size (*n*) for each experimental group/condition, given as a discrete number and unit of measurement (animals, litters, cultures, etc.)
☐	☒	A description of how samples were collected, noting whether measurements were taken from distinct samples or whether the same sample was measured repeatedly
☐	☒	A statement indicating how many times each experiment was replicated
☐	☒	The statistical test(s) used and whether they are one- or two-sided (note: only common tests should be described solely by name; more complex techniques should be described in the Methods section)
☒	☐	A description of any assumptions or corrections, such as an adjustment for multiple comparisons
☐	☒	The test results (e.g. *P* values) given as exact values whenever possible and with confidence intervals noted
☐	☒	A clear description of statistics including central tendency (e.g. median, mean) and variation (e.g. standard deviation, interquartile range)
☐	☒	Clearly defined error bars

See the web collection on statistics for biologists for further resources and guidance.

Software

Policy information about availability of computer code

7. Software

Describe the software used to analyze the data in this study.	Imaris 8.3, ImageJ and OriginPro softwares have been used in this study

For manuscripts utilizing custom algorithms or software that are central to the paper but not yet described in the published literature, software must be made available to editors and reviewers upon request. We strongly encourage code deposition in a community repository (e.g. GitHub). *Nature Methods* guidance for providing algorithms and software for publication provides further information on this topic.

Materials and reagents

Policy information about availability of materials

8. Materials availability

Indicate whether there are restrictions on availability of unique materials or if these materials are only available for distribution by a for-profit company.	No restrictions of materials availability

9. Antibodies

Describe the antibodies used and how they were validated for use in the system under study (i.e. assay and species).	N/A

10. Eukaryotic cell lines

a. State the source of each eukaryotic cell line used.	All yeast strains are sourced from ATCC as described in material and methods
b. Describe the method of cell line authentication used.	N/A
c. Report whether the cell lines were tested for mycoplasma contamination.	N/A
d. If any of the cell lines used are listed in the database of commonly misidentified cell lines maintained by ICLAC, provide a scientific rationale for their use.	N/A

Animals and human research participants

Policy information about studies involving animals; when reporting animal research, follow the ARRIVE guidelines

11. Description of research animals

Provide details on animals and/or animal-derived materials used in the study.	N/A

Policy information about studies involving human research participants

12. Description of human research participants

Describe the covariate-relevant population characteristics of the human research participants.	N/A